Negative differential transmission in graphene

B. Y. Sun and M. W. Wu*

Hefei National Laboratory for Physical Sciences at Microscale and Department of Physics, University of Science and Technology of China, Hefei, Anhui, 230026, China

(Received 4 August 2013; revised manuscript received 31 October 2013; published 17 December 2013)

By using the Kubo linear response theory with the Keldysh Green function approach, we investigate the mechanism leading to the negative differential transmission in a system with the equilibrium electron density much smaller than the photon-excited one. It is shown that the negative differential transmission can appear at low probe-photon energy (in the order of the scattering rate) or at high energy (much larger than the scattering rate). For the low probe-photon energy case, the negative differential transmission is found to come from the increase of the intraband conductivity due to the large variation of electron distribution after the pumping. As for the high probe-photon energy case, the negative differential transmission is shown to tend to appear with the hot-electron temperature being closer to the equilibrium one and the chemical potential higher than the equilibrium one but considerably smaller than half of the probe-photon energy. We also show that this negative differential transmission can come from both the inter- and the intraband components of the conductivity. Especially, for the interband component, its contribution to the negative differential transmission is shown to come from both the Hartree-Fock self-energy and the scattering. Furthermore, the influence of the Coulomb-hole self-energy is also addressed.

DOI: 10.1103/PhysRevB.88.235422 PACS number(s): 78.67.Wj, 71.10.−w, 42.65.Re, 72.80.Vp

I. INTRODUCTION

Graphene is an easily accessible, truly two-dimensional system which is attractive from the point of view of both basic physics and possible applications. In the past decade, it has attracted immense investigations.[1–12] Among these works, the time-resolved optical pump-probe measurement is widely used to investigate the dynamics of electrons in graphene.[13–32] With this method, a pump pulse is used to excite electrons from the valence band to the conduction one and then a time-delayed probe pulse with the probe-photon energy ω is applied to detect the differential transmission (DT). The experimentally obtained DT under a probe-photon energy much higher than twice of the Fermi energy is often positive with its fast relaxation of several hundred femtoseconds followed by a slower picosecond relaxation.[13,20,21,26] From the DT, the conductivity $\sigma(\omega)$ is extracted. Moreover, if ω is also much larger than the scattering rate and the electrons are considered to be free, the conductivity is given by ($\hbar \equiv 1$)[13,33,34]

$$\sigma(\omega) \approx \sigma_{\text{free}}(\omega) = -\sigma_0[f_{\mathbf{k}_\omega,1} - f_{\mathbf{k}_\omega,-1}], \tag{1}$$

in which $\sigma_0 = e^2/4$, $f_{\mathbf{k}_\omega,\eta}$ is the electron distribution with $\eta = 1$ (-1) representing the conduction (valence) band, and $k_\omega = \omega/(2\hbar v_F)$ stands for the resonant absorption state. With this equation and the temporal evolution of $\sigma_{\text{free}}(\omega)$, the evolution of the electron distribution difference at the resonant absorption state $f_{\mathbf{k}_\omega,-1} - f_{\mathbf{k}_\omega,1}$ is directly detected.

In addition to the positive DT, the negative DT, which indicates the increase of the conductivity after the pumping (positive differential conductivity), has also been observed in different experiments.[14,15,18,24,27] Sun *et al*. reported a negative DT in a system of very high equilibrium Fermi energy, with the probe-photon energy being lower than twice of the Fermi energy.[14] Soon after that, the negative DT was also observed by George *et al*. in the case where the probe-photon energy is as low as tens of meV.[15] These two kinds of negative DT can be well understood theoretically. By considering the interband conductivity of free electrons [Eq. (1)], the negative DT reported by Sun *et al*.[14] is shown to come from the weakening of the Pauli blocking due to the heating of electrons by the pump pulse.[35] As for the case with low probe-photon energy,[15] the heating of the electrons can still contribute to the negative DT.[25,36] Nevertheless, with the scattering taken into consideration, the intraband conductivity was found to be also important for the negative DT.[15,25]

In contrast to the previous two cases with moderate or small probe-photon energies, the negative DT has also been observed with the probe-photon energy being very high (e.g., >1.5 eV).[19,22,24,27,30] The mechanisms lead to this kind of negative DT is still unclear. At such high probe-photon energy, the Fermi surface is less possible to be as high as half of the probe-photon energy and hence the weakening of the Pauli blocking is less important. As for the intraband conductivity, its strength is largely suppressed and hence whether it is strong enough to lead to the negative DT is unclear. Moreover, in previous works investigating problems of the negative DT, the scattering strength used was assumed to be constant.[25] With constant scattering strength, the interband conductivity cannot lead to the negative DT. Nevertheless, with the variation of the scattering strength taken into consideration, whether it can lead to negative DT is still unknown. In addition, the variation of the Coulomb self-energy after the pumping was also suggested to be the mechanism leading to the increase of the interband conductivity and hence the negative DT.[19,24,27] However, whether it is strong enough to lead to a negative DT has not been fully theoretically demonstrated and it is even claimed that the negative DT itself may come from external factors.[30]

In this work we calculate the optical conductivity based on the linear response theory with the Keldysh Green function approach[37,38] by taking into account the contribution of the electron-phonon and the electron-impurity scatterings as well as the Coulomb self-energy explicitly. We show that for graphene with low equilibrium electron density without the

Coulomb-hole (CH) self-energy,[39,40] the negative DT can appear when the probe-photon energy ω is low (in the order of the scattering rate) or when ω is high (much larger than the scattering rate). For the low ω case, the negative DT mainly comes from the large increase of the intraband conductivity after the pumping due to the large variation of the electron distribution. As for the high ω case, the negative DT is shown to tend to appear when the hot-electron temperature T_e is close to the equilibrium one and the chemical potential is higher than the equilibrium chemical potential but considerably lower than $\omega/2$. This negative DT is found to come from the variation of both the intra- and the interband components of the conductivity. Especially, for the interband conductivity, we find that both the scattering and the Hartree-Fock (HF) self-energy can cause the negative DT.[41] In addition, the influence of CH self-energy is also addressed.

This paper is organized as follows. In Sec. II we set up the model and lay out the formalism. In Sec. III the results obtained numerically are presented. We summarize and discuss in Sec. IV.

II. MODEL AND FORMALISM

The effective Hamiltonian of graphene near the K and K' points can be described by[42]

$$H_0 = \sum_{\mathbf{k}s\mu\eta} \eta\varepsilon_{\mathbf{k}} c^{\dagger}_{\mathbf{k}s\eta\mu} c_{\mathbf{k}s\eta\mu}. \tag{2}$$

Here $\mu = 1$ (-1) stands for K (K') valley, $\eta = 1$ (-1) represents conduction (valence) band, s denotes spin, and $\varepsilon_{\mathbf{k}} = v_F k$ with v_F being the Fermi velocity. In this work we only investigate the linearly polarized normal incident light with the electric field along $\hat{\mathbf{x}}$ direction. Then, based on the effective Hamiltonian, the current operator reads (the in-plane photon momentum $q = 0$)[34]

$$\hat{\mathbf{j}} = \sum_{\mathbf{k}s\mu\eta\eta'} d^{\mu}_{\theta_{\mathbf{k}}\eta\eta'} c^{\dagger}_{\mathbf{k}s\eta\mu} c_{\mathbf{k}s\eta'\mu}, \tag{3}$$

with the dipole matrices being

$$d^{\mu}_{\theta_{\mathbf{k}}\eta\eta'} = -|e| v_F [\eta' e^{i\mu\theta_{\mathbf{k}}} + \eta e^{-i\mu\theta_{\mathbf{k}}}]/2. \tag{4}$$

It has been shown that the hot-electron Fermi distribution is quickly established after the pumping with the hot-electron temperatures in the conduction and valence bands being the same while the chemical potentials being different.[18,43] Based on this result, the electron density matrix without interactions is set to be $\rho_0 = \exp[-\sum_{\mathbf{k}s\mu\eta} \beta_e(\eta\varepsilon_{\mathbf{k}} - \mu_\eta) c^{\dagger}_{\mathbf{k}s\eta\mu} c_{\mathbf{k}s\eta\mu}]$, with μ_η being the chemical potential in band η, $\beta_e = k_B T_e$, and T_e standing for the electron temperature. Then, from the Kubo formula with the Keldysh Green function approach, the optical conductivity is expressed as[33,37,38,44]

$$\sigma(\omega) = \int d\mathbf{k} \int d\omega_1 g_d \sum_{\eta\eta'} d^{\mu}_{\theta_{\mathbf{k}}\eta\eta'} d^{\mu}_{\theta_{\mathbf{k}}\eta'\eta} A(\mathbf{k},\eta',\omega_1+\omega) \times A(\mathbf{k},\eta,\omega_1)[F(\omega_1,\eta) - F(\omega_1+\omega,\eta')]/(16\pi^3\omega). \tag{5}$$

Here $g_d = 4$ comes from the valley and spin degeneracies and $F(\omega,\eta) = \{\exp[(\omega - \mu_\eta)/(k_B T_e)] + 1\}^{-1}$. In this equation, the two band indices η and η' in $[F(\omega_1,\eta) - F(\omega_1+\omega,\eta')]$ can be used to distinguish the contributions of the intra- and interband conductivities. The intraband conductivity is defined as terms with $\eta = \eta'$ and the interband one with $\eta \neq \eta'$. With this definition of the inter- and intraband conductivities, their differential conductivities are defined as the difference of the corresponding conductivities after and before the pumping. The electron spectral function is given by

$$A(\mathbf{k},\eta,\omega) = -2\mathrm{Im}\{[\omega - \eta\varepsilon_{\mathbf{k}} - \Sigma^{\mathrm{R}}(\mathbf{k},\eta,\omega)]^{-1}\}. \tag{6}$$

Here $\Sigma^{\mathrm{R}}(\mathbf{k},\eta,\omega)$ represents the retarded self-energy from the electron-electron, electron-phonon, and electron-impurity interactions. The self-energy from the electron-impurity scattering is calculated from[34]

$$\Sigma_{\mathrm{i}}(k) = -\frac{i\pi n_i}{2} \int \frac{d^2k'}{(2\pi)^2} \left(\frac{V_{\mathbf{k}'-\mathbf{k}}}{\epsilon_{\mathbf{q}}}\right)^2 \delta(\varepsilon_{\mathbf{k}} - \varepsilon_{\mathbf{k}'}) \times [1 - \cos(\theta_{\mathbf{k}} - \theta_{\mathbf{k}'})][1 + \cos(\theta_{\mathbf{k}} - \theta_{\mathbf{k}'})]. \tag{7}$$

Here $\epsilon_{\mathbf{q}}$ is the dielectric function calculated as Scharf *et al.*[34] and $V_{\mathbf{q}} = 2\pi e^2/(\kappa q)$ represents the two-dimensional bare Coulomb potentials with κ standing for the background dielectric constant.[34]

For the self-energy from the electron-phonon scattering, although the temperatures of electrons and phonons can be different, the Feynman rules and diagrammatic technique for the Keldysh Green function approach are still valid.[44] With this approach, the retarded self-energy is obtained as

$$\Sigma^{\mathrm{R}}_{\mathrm{ph}}(\mathbf{k},\eta,\omega) = \sum_{\mathbf{q},\eta',\lambda} M_{\eta,\eta',\lambda}(\mathbf{k}-\mathbf{q},\mathbf{q}) M_{\eta'\eta,\lambda}(\mathbf{k},-\mathbf{q}) \times \left[\frac{n_{\mathbf{q}\lambda} + 1 - F(\epsilon_{|\mathbf{k}-\mathbf{q}|},\eta')}{\omega + i0^+ - \eta'\epsilon_{|\mathbf{k}-\mathbf{q}|} - \omega_\lambda(\mathbf{q})} + \frac{n_{\mathbf{q}\lambda} + F(\epsilon_{|\mathbf{k}-\mathbf{q}|},\eta')}{\omega + i0^+ - \eta'\epsilon_{|\mathbf{k}-\mathbf{q}|} + \omega_\lambda(\mathbf{q})}\right]. \tag{8}$$

Here $M_{\eta,\eta',\lambda}(\mathbf{k},-\mathbf{q})$ are the electron-phonon scattering matrices for phonons in branch λ with their detailed forms given by Scharf *et al.*[34]; $n_{\mathbf{q}\lambda} = \{\exp[\omega_{q,\lambda}/(k_B T_{\mathrm{ph}})] - 1\}^{-1}$ is the distribution for phonons with energy $\omega_{q,\lambda}$ and temperature T_{ph}. In the following we ignore the effect of polaronic shifts, i.e., the real part of the electron-phonon self-energy and compensate such approximation by renormalizing the spectral function to fulfill $\int d\omega A(\mathbf{k},\eta,\omega) = 2\pi$ as done by Scharf *et al.*[34]

As for the self-energy from the Coulomb interaction, we take into account the HF self-energy[39]

$$\Sigma^{\mathrm{HF}}_{\mathbf{k},\eta} = \sum_{\mathbf{k}'} -\eta\cos(\theta_{\mathbf{k}} - \theta_{\mathbf{k}'}) \frac{V_{\mathbf{k}'-\mathbf{k}}}{2\epsilon_{\mathbf{k}'-\mathbf{k}}} \left(f^e_{\mathbf{k}'} + f^h_{\mathbf{k}'}\right). \tag{9}$$

Here $f^e_{\mathbf{k}} = F(\varepsilon_{\mathbf{k}},1)$ and $f^h_{\mathbf{k}} = 1 - F(-\varepsilon_{\mathbf{k}},-1)$ are the electron and hole distributions, respectively. This self-energy comes from the Coulomb exchange self-energy[45–47]

$$\hat{\Sigma}_{\mathrm{ee}}(\mathbf{k},\eta,\omega) = -\frac{1}{2}\sum_{\mathbf{k}'\eta'} [1 + \eta\eta'\cos(\theta_{\mathbf{k}} - \theta_{\mathbf{k}'})] \times F(\eta' v_F \mathbf{k}',\eta') V_{\mathbf{k}'-\mathbf{k}}/\epsilon_{\mathbf{k}'-\mathbf{k}}, \tag{10}$$

with the exchange term of the full valence band subtracted as it is already included in the original single-particle energy.[41]

However, it is known in semiconductor optics that there is a Debye shift or the CH self-energy in addition to the HF self-energy, which is expressed as[39,40,48]

$$\Sigma^{\mathrm{CH}}_{\mathbf{k},\eta} = \sum_{\mathbf{q}} \eta \cos(\theta_{\mathbf{k}} - \theta_{\mathbf{k}+\mathbf{q}}) V_{\mathbf{q}} \left(1/\epsilon_{\mathbf{q}} - 1/\epsilon^0_{\mathbf{q}}\right)/2, \quad (11)$$

with $\epsilon^0_{\mathbf{q}}$ representing the dielectric function at $T_e = 0$ K and $\mu_1 = \mu_{-1} = 0$ meV. The physics of this CH self-energy is as follows. After the pumping, the pump-excited electrons change the screening strength. As a result, the subtracted exchange term of the full valence band also varies [Eq. (11)]. It has been shown in semiconductor optics that the CH self-energy leads to a strong renormalization of the band structure (band-gap shrinkage).[40,48] Due to the similar renormalization of the band structure in graphene, it was speculated that this variation of the Coulomb self-energy is responsible for the negative DT.[27] In this work, we also calculate the influence of the Coulomb self-energy to check this speculation.

III. RESULTS

From the relation between the transmission and conductivity[13,49–51]

$$T_\omega = |1 + N_{\mathrm{lay}}\sigma(\omega)\sqrt{\mu_0/\epsilon_0}/(1 + n_{\mathrm{ref}})|^{-2}, \quad (12)$$

one finds that the negative DT emerges when the optical conductivity increases after the pumping. Therefore, instead of calculating the DT, we investigate the variation of the conductivity before and after the pulse (differential conductivity) $\Delta\sigma(T_e,\mu_1,\mu_{-1},\omega) = \sigma(T_e,\mu_1,\mu_{-1},\omega) - \sigma(T_0,\mu^0_1,\mu^0_{-1},\omega)$. Here, for electrons before the pumping, we choose their temperature $T_0 = 300$ K. We concentrate on the case with the photon-excited electron density much larger than the equilibrium one and hence choose the chemical potential $\mu^0_1 = \mu^0_{-1} = 0$ for convenience. Then, due to the symmetry between electrons and holes, one always has $\mu_1 = -\mu_{-1}$ after the establishment of the Fermi distribution. Unlike some earlier theoretical works claiming that μ_1 is always zero,[52–56] our recent work[35] shows that μ_1 is nonzero when the Fermi distribution is established. This is because of the static screening used in these works.[52,53,56] With the static screening, the strong interband scattering due to the Auger process drives the electrons and holes to the quasiequilibrium state very quickly and leads to an equilibrium electron-hole Fermi distribution (i.e., $\mu_1 = 0$). However, we have shown that in graphene the screening should be the dynamic one which forbids the Auger process adopted in the previous works.[57–60] As a result, the interband scattering process is much weaker and the Fermi distributions are established *separately* for electrons and holes.[35] This conclusion is also supported by the experimental results by Breusing *et al.*[18] It is further noted that this result is also consistent with that in semiconductor optics dealing with the quasiequilibrium electron-hole plasma,[61–63] where the interband scattering is also weak. Based on these considerations, in this work, we will vary the value of μ_1 to investigate its influence. In our calculation, the material parameters are the same as in Ref. 34 and the impurity density $n_i = 5 \times 10^{11}$ cm^{-2}. The temperature of phonons T_{ph} is chosen to be the same as electrons and the substrate is chosen to be SiO_2 unless otherwise specified. It is noted that we restrict our investigation with the probe-photon energy ω being lower than 2000 meV. Hence the energies of the electron states affecting the conductivities are mainly lower than 1000 meV, where the linear spectrum approximation is sound.[9,64]

A. Contributions of intra- and interband differential conductivities

In this section we first give an analytical analysis on the intra- and interband components of the conductivity and then show their contributions to the total differential conductivity numerically.

1. *Analytical analysis on the intra- and interband conductivities*

The increase of the total conductivity after pumping may come from both the intra- and the interband components of the conductivity. For the intraband component in Eq. (5), it can be simplified by assuming the self-energy $\Sigma^{\mathrm{R}}(\mathbf{k},\eta,\omega) = \mathrm{Re}\Sigma_{\mathbf{k},\eta} + i/(2\tau)$. Furthermore, by using the condition $\mu_1 = -\mu_{-1}$ and taking the limit $\omega \to 0$, one has

$$\sigma_{\mathrm{intra}}(\omega) = e^2\tau D(T_e,\mu_1,\mu_{-1})/[\pi(1+\omega^2\tau^2)]. \quad (13)$$

Here $\mathrm{Re}\Sigma_{\mathbf{k},\eta}$ is the real part of the self-energy which comes from the HF and CH self-energies and

$$\begin{aligned} D(T_e,\mu_1,\mu_{-1}) &= 2\int_0^\infty d\varepsilon\varepsilon[-\partial_\varepsilon F(\varepsilon + \mathrm{Re}\Sigma_{\mathbf{k},1},1)] \\ &= 2\int_{\frac{-\mu'}{k_B T_e}}^\infty dx(k_B T_e x + \mu')\frac{e^x}{(e^x+1)^2}, \end{aligned} \quad (14)$$

with $\mu' = \mu_1 - \mathrm{Re}\Sigma_{\mathbf{k},1}$. From Eq. (13), one finds that the increase of the scattering strength, i.e., the decrease of τ, leads to the increase (decrease) of the conductivity when the probe-photon energy ω is larger (smaller) than τ^{-1}. Moreover, from Eqs. (13) and (14), it is found that the increase of the electron temperature T_e and chemical potential μ_1 as well as the decrease of the self-energy $\mathrm{Re}\Sigma_{\mathbf{k},1}$ lead to the increase of $D(T_e,\mu_1,\mu_{-1})$ and hence σ_{intra}.

As for the interband conductivity, its increase may come from the variations of the scattering (the imaginary part of the self-energy), the HF self-energy, and the CH self-energy (the real part of the self-energy). For the scattering, it can be shown that the interband conductivity increases with the decrease of the scattering strength.[65] Therefore, the positive differential conductivity may appear when the scattering strength decreases. On the other hand, for the HF and CH self-energies, their influences are understood from the simplified Eq. (5) by neglecting the electron-impurity and electron-phonon scatterings:

$$\begin{aligned} \sigma(\omega) &= \frac{g_d\sigma_0 v_F^2}{\omega}\int_0^\infty dkk\delta\left(\omega - 2\varepsilon_{\mathbf{k}} + \Sigma^{\mathrm{ee}}_{\mathbf{k},-1} - \Sigma^{\mathrm{ee}}_{\mathbf{k},1}\right) \\ &\quad\times\left[F\left(-\varepsilon_{\mathbf{k}} + \Sigma^{\mathrm{ee}}_{\mathbf{k},-1},-1\right) - F\left(\omega - \varepsilon_{\mathbf{k}} + \Sigma^{\mathrm{ee}}_{\mathbf{k},-1},1\right)\right] \\ &= \left[F\left(-\varepsilon_{\mathbf{k}_\omega} + \Sigma^{\mathrm{ee}}_{\mathbf{k}_\omega,-1},-1\right) - F\left(\omega - \varepsilon_{\mathbf{k}_\omega} + \Sigma^{\mathrm{ee}}_{\mathbf{k}_\omega,-1},1\right)\right] \\ &\quad\times g_d\sigma_0 v_F^2 k_\omega \Big/ \left\{\omega\left[2v_F - \partial_k\left(\Sigma^{\mathrm{ee}}_{\mathbf{k}_\omega,-1} - \Sigma^{\mathrm{ee}}_{\mathbf{k}_\omega,1}\right)\right]\right\}. \end{aligned} \quad (15)$$

Here k_ω satisfies $\omega - 2\varepsilon_{\mathbf{k}_\omega} + \Sigma^{\mathrm{ee}}_{\mathbf{k}_\omega,-1} - \Sigma^{\mathrm{ee}}_{\mathbf{k}_\omega,1} = 0$ and $\Sigma^{\mathrm{ee}}_{\mathbf{k}_\omega,\eta}$ stands for the corresponding self-energy from the Coulomb interaction (HF and CH self-energies). After the pumping,

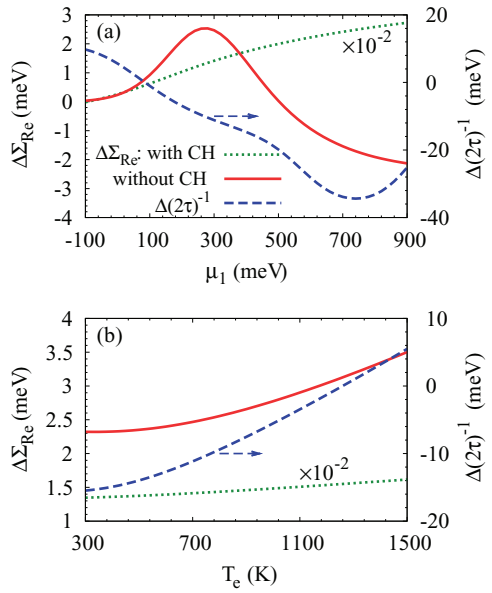

FIG. 1. (Color online) (a) Chemical potential and (b) electron temperature dependencies of $\Delta\Sigma_{\rm Re}$ and $\Delta(2\tau)^{-1}$ with and without the CH self-energy. Here the probe-photon energy ω is chosen to be 1500 meV. For the chemical potential μ_1 dependence, the electron temperature $T_e = 700$ K and for the electron temperature dependence, the chemical potential $\mu_1 = 300$ meV. Moreover, to make the results clearer, the curves with the CH self-energy plotted in the figure are $\Delta\Sigma_{\rm Re}/100$. Note that the scale of $\Delta(2\tau)^{-1}$ is on the right-hand side of the frame.

the difference of the HF self-energy $\Sigma^{\rm HF}_{\mathbf{k}_\omega,-1} - \Sigma^{\rm HF}_{\mathbf{k}_\omega,1}$ may overcome the decrease from the increasing screening strength and increase due to the increase of the carrier density [Eq. (9)]. Moreover, the difference of the CH self-energy $\Sigma^{\rm CH}_{\mathbf{k}_\omega,-1} - \Sigma^{\rm CH}_{\mathbf{k}_\omega,1}$ can also increase due to the enhancement of the screening strength. As a result, k_ω may increase, which tends to enhance the interband conductivity.

2. *Numerical investigation on the contributions of intra- and interband differential conductivities*

Since the variations of $\Sigma^{\rm HF}_{\mathbf{k}_\omega,-1} - \Sigma^{\rm HF}_{\mathbf{k}_\omega,1}$ and $(2\tau)^{-1}$ after the pumping are highly related to the interband differential conductivity as discussed in the previous subsection, we first investigate their properties as a guidance. We calculate their variations as $\Delta\Sigma_{\rm Re} = \Sigma^{\rm HF}_{\mathbf{k}_\omega,-1} - \Sigma^{\rm HF}_{\mathbf{k}_\omega,1} - \Sigma^{\rm HF,0}_{\mathbf{k}_\omega,-1} + \Sigma^{\rm HF,0}_{\mathbf{k}_\omega,1}$ and $\Delta(2\tau)^{-1} = (2\tau)^{-1} - (2\tau_0)^{-1}$, with $\Sigma^{\rm HF,0}_{\mathbf{k}_\omega,-1}$, $\Sigma^{\rm HF,0}_{\mathbf{k}_\omega,1}$ and $(2\tau_0)^{-1}$ obtained before the pumping. Here $(2\tau)^{-1}$ is calculated from the imaginary part of the retarded self-energy $(2\tau)^{-1} = |{\rm Im}\Sigma^{\rm R}(\mathbf{k}_\omega,1,\bar{\omega})|$, with $\bar{\omega} = v_F k_\omega$. Moreover, the temperature of phonons are set to be the same as that of electrons. Then, the chemical potential and electron temperature dependencies of $\Delta\Sigma_{\rm Re}$ and $\Delta(2\tau)^{-1}$ are plotted in Figs. 1(a) and 1(b), respectively. From Fig. 1(a) one finds that for $\Delta\Sigma_{\rm Re}$ without the CH self-energy, it is positive when $\mu_1 < 500$ meV and a peak appears around $\mu_1 = 280$ meV. Since the positive $\Delta\Sigma_{\rm Re}$ tends to increase the differential conductivity (i.e., decrease the DT) as discussed in Sec. III A 1, this positive $\Delta\Sigma_{\rm Re}$ with the peak shown in the figure indicates that the increase of the carrier densities can lead to the negative DT unless the chemical potential is so large that the decrease of $\Delta\Sigma_{\rm Re}$ due to the increase of the screening strength becomes dominant. Moreover, one also finds that $\Delta(2\tau)^{-1}$ shows a valley in the μ_1 dependence. This indicates that a peak of the differential conductivity in the μ_1 dependence can occur, since the decrease of the scattering strength tends to enhance the differential conductivity. As for the electron temperature T_e dependencies of $\Delta(2\tau)^{-1}$ and $\Delta\Sigma_{\rm Re}$ without the CH self-energy as shown in Fig. 1(b), one finds that both of them increase with the increase of temperature in the parameter range investigated here. This indicates that the HF self-energy tends to enhance the differential conductivity but the scattering tends to suppress it with the increase of temperature. In addition to the case without the CH self-energy, we also show $\Delta\Sigma_{\rm Re}$ with the CH self-energy in the figures. It is found that the corresponding $\Delta\Sigma_{\rm Re}$ increases monotonically with the increase of μ_1 and T_e. Moreover, its value is much larger than the one without the CH self-energy. Hence, one expects that the differential conductivity is markedly enhanced by the CH self-energy.

We then numerically calculate the probe-photon energy dependence of the total differential conductivity. The case without the CH self-energy is first investigated. It is noted that the chemical potential μ_1 and temperature T_e of hot electrons vary with the temporal evolution after the pumping. Here we take $T_e = 500$ K and $\mu_1 = -\mu_{-1} = 300$ meV as an example to investigate the possible mechanisms discussed in Sec. III A 1. The total differential conductivity as function of probe-photon energy is plotted in Fig. 2(a) (red solid curve). To identify the individual contributions of inter- and intraband components, we also plot the differential conductivity with only the interband component in the figure (open squares). One finds that, at very low probe-photon energy ω (<50 meV), the total differential conductivity is positive and far away from zero, while the interband differential conductivity is negative. This indicts that the large positive differential conductivity at low ω comes from the intraband component.

As analyzed in Sec. III A 1, this large positive intraband differential conductivity at low probe-photon energy ω comes from the variation of $D(T_e,\mu_1,\mu_{-1})$ and τ after the pumping. The variation of $D(T_e,\mu_1,\mu_{-1})$ can be obtained from Eq. (14) if the electron distribution (i.e., T_e and μ_1) and the HF self-energy ${\rm Re}\Sigma_{\mathbf{k},1}$ are known. It is noted that ${\rm Re}\Sigma_{\mathbf{k},1}$ for the temperatures and chemical potentials calculated here is always less than 3 meV, much smaller than the chemical potential after the pumping (300 meV). Hence, the influence of the HF self-energy on $D(T_e,\mu_1,\mu_{-1})$ can be neglected and one obtains $D(T_e,\mu_1,\mu_{-1}) = 35.8$ and 600 meV for the cases before and after the pumping, respectively. To further identify the contribution of τ, we fit the total conductivity in the region $\omega < 50$ meV with

$$\tilde{\sigma}(\omega) = \sigma_{\rm intra}(\omega) + \sigma_{\rm free}(\omega). \tag{16}$$

Here $\sigma_{\rm free}(\omega)$ is included to take into account the influence of the interband conductivity. τ is fitted to be 0.07 and 0.17 meV^{-1} for the cases before and after pumping, respectively [the obtained differential conductivity is plotted in Fig. 2(a) as the green dotted curve]. One finds that the relative change of τ is much smaller than that of $D(T_e,\mu_1,\mu_{-1})$. Hence the variation of the intraband conductivity mainly comes from

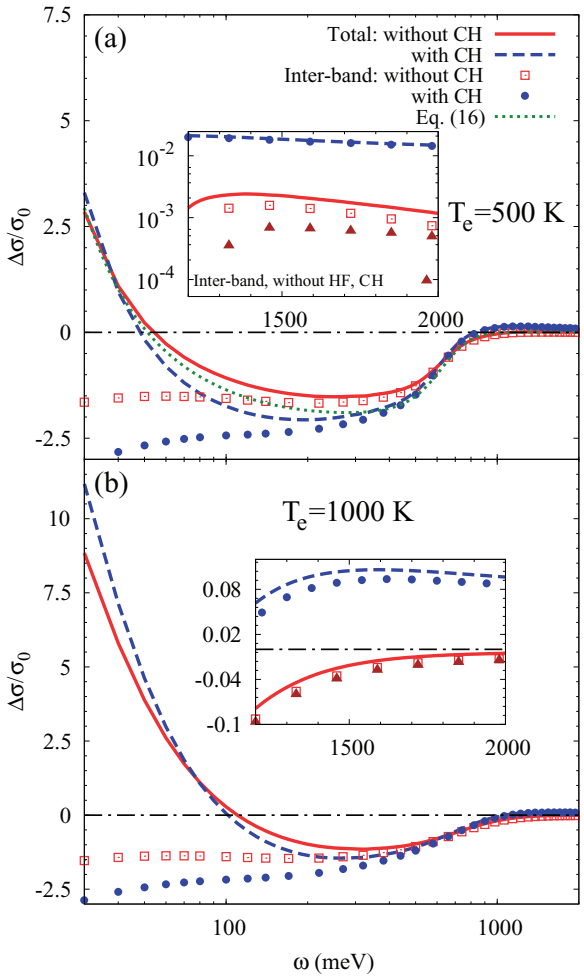

FIG. 2. (Color online) Interband as well as total differential conductivities with and without the CH self-energy as function of the probe-photon energy ω. The states after the pumping are chosen to be (a) $T_e = 500$ K and $\mu_1 = -\mu_{-1} = 300$ meV, and (b) $T_e = 1000$ K and $\mu_1 = -\mu_{-1} = 300$ meV. The total conductivity without the CH self-energy in (a) is fitted for $\omega \leqslant 50$ meV by Eq. (16) with the fitted results plotted as the green dotted curve. The inset zooms the range at high ω with the interband differential conductivity without the CH and HF self-energies plotted as brown solid triangles. The black chain line in the figure marks $\Delta\sigma/\sigma_0 = 0$.

the variation of the electron distribution, which leads to the huge increase of $D(T_e,\mu_1,\mu_{-1})$. Moreover, since the influence of the HF self-energy on $D(T_e,\mu_1,\mu_{-1})$ can be neglected, its influence on the intraband component of the differential conductivity is also marginal. It is further noted from the figure that, with the increase of the probe-photon energy ω from zero, $\Delta\sigma$ decreases fast and becomes negative around $\omega = 55$ meV. This quick decrease of $\Delta\sigma$ can be understood from Eq. (13), which infers that the influence of the intraband component of the differential conductivity is significant only when ω is in the order of τ^{-1}.

In addition to the large positive differential conductivity shown in the case of low probe-photon energy ω, another small positive total differential conductivity also appears when ω is high (larger than 1200 meV) as shown by the red solid curve in the inset. One also finds from the inset that the interband differential conductivity (open squares) is also positive. Moreover, it is smaller than the total one with their difference being in the same order ($\sim 10^{-3}\sigma_0$) as the interband differential conductivity. This means that the positive total differential conductivity comes from both the inter- and the intraband components and both contributions are important at such high ω.

For the positive contribution from the intraband component at such high ω, it still mainly comes from the large variation of the electron distribution after the pumping as the case with low probe-photon energy ω. This is confirmed by calculating the intraband component in Eq. (5) with the distribution $[F(\omega_1,\eta) - F(\omega_1+\omega,\eta)]$ fixed with the pumping. We find that the obtained intraband conductivity decreases more than 75% for all ω shown in the inset (not plotted in the figure).

As for the positive contribution from the interband component, it may come from the variations of both the HF self-energy and the scattering strength after pumping as discussed in Sec. III A 1. Although the influence of the HF self-energy on the intraband component is marginal, it may have non-negligible influence on the interband component. To further identify its contribution, we also plot the interband differential contribution without the HF self-energy in the inset (brown solid triangles). One finds that the one with the HF self-energy is about 2–3 times of that without the HF self-energy. This means that the variations of both the HF self-energy and the scattering strength have important contributions to the positive interband differential conductivity at such high probe-photon energy.

We further investigate the influence of the CH self-energy on the differential conductivity. With the CH self-energy, the total differential conductivity and the one with only interband component are plotted as the blue dashed curve and the blue solid dots in the figure, respectively. One finds that their qualitative behaviors are similar to those without the CH self-energy, i.e., the large positive differential conductivity from the intraband component at low probe-photon energy ω as well as the emergence of positive differential conductivity at high ω. Nevertheless, it is seen that the differential conductivity with the CH self-energy included varies markedly compared with the one without the CH self-energy. This means that the CH self-energy has pronounced influence on the differential conductivity, which is consistent with the large positive $\Delta\Sigma_{\mathrm{Re}}$ with the CH self-energy shown in Fig. 1. Moreover, it is also seen that with the CH self-energy, the total and the interband differential conductivities are very close at high ω as shown in the inset. This indicates that the large influence of the CH self-energy at high ω is mainly on the interband component.

To further show the influence of T_e, we plot the probe-photon energy ω dependence of the differential conductivities at the electron temperature $T_e = 1000$ K and chemical potential $\mu_1 = 300$ meV in Fig. 2(b). For the case without the CH self-energy, the total differential conductivity (red solid curve) at high ω (>1200 meV as shown in the inset) becomes negative, which is different from the case at $T_e = 500$ K. To show the origin of this negative differential conductivity, we plot the interband one with (red open squares) and without (brown solid triangles) the HF self-energy in the inset. It is shown that they are also negative and the total differential conductivity is close to the interband one without the HF self-energy. This indicates

that the negative total differential conductivity comes from the negative interband differential conductivity without the CH and HF self-energies under high temperature at high ω. To see the influence of the CH self-energy, we plot in the inset both the total (blue dashed curve) and the interband (blue solid dots) differential conductivities. One finds both become positive for the high ω case. This again shows that the CH self-energy has a large influence on the differential conductivity.

B. Condition for negative DT

In the previous section, the mechanisms and their contributions to the positive differential conductivity are investigated under specific electron temperatures T_e and chemical potential μ_1. However, the hot-electron temperature and the chemical potential after the pumping vary with time. Here we investigate the conditions of T_e and μ_1 as well as the probe-photon energy ω for the emergence of the positive differential conductivity (i.e., negative DT). Since the positive differential conductivity in the low ω case has been shown to come from the intraband component of the conductivity, in this section, we only investigate the case with high ω, where the negative DT was speculated to come from the scattering and the Coulomb self-energy.[19,24,27] The cases without the CH self-energy are first studied with the total differential conductivity in the ω-μ_1 parameter space plotted in Fig. 3(a). Here the electron temperature is chosen to be 700 K, which is among those estimated in the experiment and the phonon temperature is chosen to be the same as that of electrons. We only plot the region with positive differential conductivity for clarity. It is found that if the probe-photon energy is larger than 1250 meV, the positive differential conductivity emerges with the corresponding range of μ_1 depending on ω. To further show the contributions of the inter- and intraband components, we plot the chemical potential dependence of the total and the interband differential conductivities in Fig. 3(b) with $\omega = 1500$ and 1700 meV. From the figure, one finds that the interband differential conductivities (open squares and dashed curve) are negative but the total conductivity is positive when $160 < \mu_1 < 420$ meV for $\omega = 1700$ meV (solid curve) and $140 < \mu_1 < 340$ meV for $\omega = 1500$ meV (dots). This indicates that the positive differential conductivity comes from the intraband component. This result is consistent with previous ones that the intraband differential conductivity increases with T_e and μ_1 [Eq. (14)], while the interband one is negative if the hot-electron temperature is much larger than the equilibrium one. Moreover, one also finds that peaks appear in the chemical potential dependencies of both the total and the interband differential conductivities with the corresponding μ_1 considerably smaller than $\omega/2$. Considering that the intraband differential conductivity increases with μ_1 monotonously, the peak shown in the total differential conductivity is understood to come from the interband one, which is consistent with the valley of $\Delta(2\tau)^{-1}$ shown in Fig. 1(a) as discussed in the first paragraph of Sec. III A 2. In addition, it is also shown in the figure that with the increase of ω, the peak of the interband differential conductivity appears at higher μ_1 (pointed by the arrows), this explains that the positive total differential conductivity tends to appear at higher μ_1 with the increases of ω as shown in Fig. 3(a). To further show the influence of the

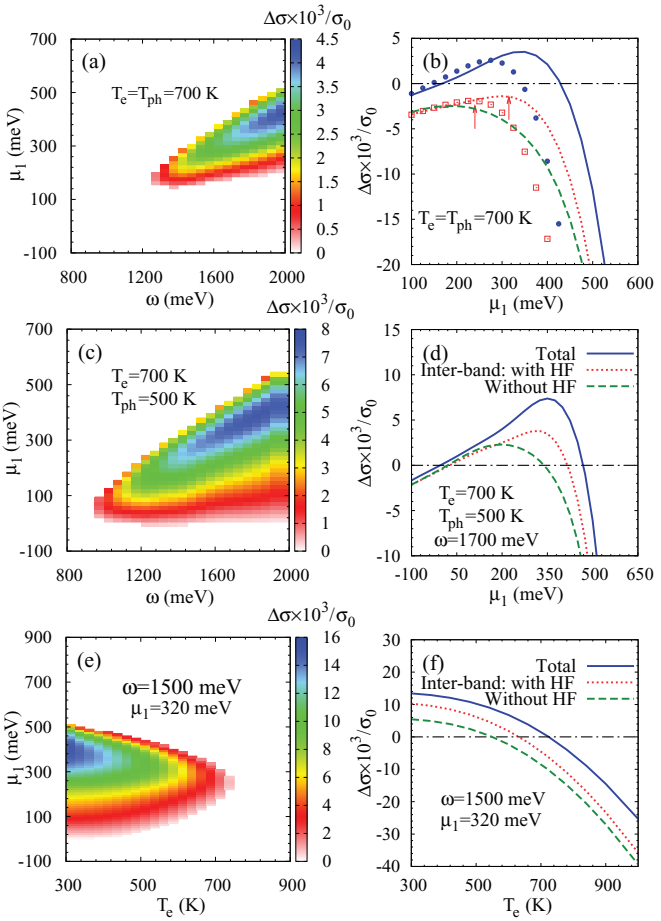

FIG. 3. (Color online) (a) Total differential conductivity in ω-μ_1 space with $T_{ph} = T_e = 700$ K. (b) Chemical potential dependence of the total differential conductivity at $\omega = 1500$ meV (blue solid dots) and 1700 meV (blue solid curve) as well as the interband one at $\omega = 1500$ meV (red open squares) and 1700 meV (red dashed curve). The chemical potential dependence of the interband differential conductivity without the HF self-energy at $\omega = 1700$ meV is also plotted as the green dashed curve. Here $T_e = T_{ph} = 700$ K. The red arrows mark the peak of the interband differential conductivities. (c) Total differential conductivity in the ω-μ_1 parameter space with T_{ph} being 200 K lower than T_e. (d) Chemical potential dependence of the total differential conductivity at $\omega = 1700$ meV as well as that for the interband one with and without the HF self-energy. Here $T_e = 700$ K and $T_{ph} = 500$ K. (e) Total differential conductivities in the T_e-μ_1 parameter space. Here $\omega = 1500$ meV and $T_{ph} = T_e$. (f) Temperature dependence of the total differential conductivity as well as that for the interband one with and without the HF self-energy. Here μ_1 is chosen to be 320 meV. For clarity, only the positive differential conductivity is plotted in (a), (c), and (e). The chain lines in (b), (d), and (f) mark $\Delta\sigma/\sigma_0 = 0$.

HF self-energy on the interband differential conductivity, we plot the interband differential conductivity at $\omega = 1700$ meV without the HF self-energy (green dashed curve) in Fig. 3(b). It is shown that the interband differential conductivities with and without the HF self-energy are close at small μ_1 (<200 meV). This is understood since the HF self-energy is small when the excited electron density is small (i.e., μ_1 is small). On the other hand, the HF self-energy becomes large when the

chemical potential after the pumping is several hundred meV larger than the equilibrium one with the screening not strong enough to suppress it. This has been shown in Fig. 1(a), where a peak occurs in the chemical potential dependence of the variation of the HF self-energy (i.e., $\Delta\Sigma_{\mathrm{Re}}$ shown by the red solid curve) around $\mu_1 = 300$ meV. One finds that the region of the peak is just the one that the HF self-energy leads to an obvious increase of the interband differential conductivity as shown in Fig. 3(b).

One also finds from Fig. 3(a) that the positive differential conductivity (negative DT) emerges only when the probe-photon energy ω is high enough. This is supported by the experimental data by Shang *et al.*[24] They showed that the negative DT appears when the probe-photon energy ω is larger than 2000 meV but disappears when ω is smaller than 1835 meV under very strong pumping strength. From the numerical results shown in Fig. 3(a) (where $T_e = 700$ K), this property can be shown by electrons with the chemical potential μ_1 around 490 meV. One finds that the corresponding differential conductivity (DT) changes from negative (positive) to positive (negative) when $\omega > 1900$ meV. It is noted that the electron density under these T_e and μ_1 is 1.9×10^{13} cm^{-2}. This electron density is also reasonable since the pumping strength used in the experiment is very strong.

It is noted that in our calculation, all modes of phonons are assumed to be at the same temperature as electrons. This is suitable when the DT is measured at the time long enough after the pumping.[20] Nevertheless, as shown in the literature,[35,43,66–69] the temperatures of phonons can be several hundred Kelvins lower than that of electrons when the hot-electron–Fermi distribution is just established. To further investigate the influence of the lower phonon temperature, we also show the results with the phonon temperature being 200 K lower than the electron temperature T_e in Fig. 3(c). It is shown that with the decrease of the phonon temperature, the region of the positive differential conductivity is enlarged. This is understood since the electron-phonon scattering strength decreases with the decrease of the phonon temperature, which increases the interband differential conductivity.[65] To confirm this, we also plot the chemical potential dependence of the total and the interband differential conductivities with $T_{\mathrm{ph}} = 500$ K and $\omega = 1700$ meV in Fig. 3(d). Compared to the one with $T_{\mathrm{ph}} = 700$ K [Fig. 3(b)], it is found that the interband differential conductivity without the HF self-energy (green dashed curve) increases markedly and it can even lead to positive differential conductivity at $45 < \omega < 350$ meV.

We further give a detailed investigation on the total differential conductivity in the electron-temperature–chemical-potential (T_e-μ_1) space at a fixed probe-photon energy $\omega = 1500$ meV. The phonon temperature is chosen to be the same as the electrons and the results are plotted in Fig. 3(e). One finds that the positive differential conductivity can appear when $T_e < 730$ K. To further identify the contributions of the inter- and intraband components, we plot the temperature dependence of the differential conductivity in Fig. 3(f) with $\mu_1 = 320$ meV. One finds that the total differential conductivity (solid curve) is obviously larger than the interband one (dotted curve). This indicates the important positive contribution of the intraband component. Moreover, it is also shown that the difference between the interband differential conductivities with (red dotted curve) and without (green dashed curve) the HF self-energy varies slowly with the temperature. This means that in the parameter range investigated here, the influence of temperature on the HF self-energy is small. In addition, it is also found that the interband differential conductivity with only scattering (i.e., without the HF self-energy) can also be positive when T_e is close to the equilibrium one (300 K). However, it decreases with the increase of the temperature quickly and becomes negative when $T_e > 550$ K.

Now, we can lay out the conditions for the emergence of the negative DT (or equivalently, positive differential conductivity) in graphene with low equilibrium electron density. The negative DT can appear both in the low probe-photon energy ω (in the order of the scattering rate) case and in the high ω case (much larger than the scattering rate). For the low ω case, this negative DT mainly comes from the increase of the intraband conductivity. This increase is mainly due to the large variation of the electron distribution after the pumping and is almost not influenced by the HF self-energy in the temperature range investigated here. As for the high ω case, although the DT for free electrons [i.e., the one with the conductivity calculated from Eq. (1)] can never be negative, the negative DT can appear if the scattering is taken into consideration. With the scattering, the interband conductivity tends to lead to a negative DT when the hot-electron temperature T_e is close to the equilibrium one and the chemical potential μ_1 is higher than the equilibrium chemical potential but considerably smaller than $\omega/2$. Moreover, this region of the negative DT determined by the interband conductivity can be further expanded by the intraband one, which always tends to decrease the DT if T_e and μ_1 increase after the pumping. Furthermore, the HF self-energy can also contribute to the negative DT by increasing the interband differential conductivity when μ_1 is much higher than the equilibrium chemical potential (about several hundred meV) but is not too high to avoid the strong suppression of the HF self-energy from the screening in the temperature range usually estimated in the experiment (around 1000 K). This further expands the region of the negative DT at high ω. We further note that if the phonon temperature is considered to be smaller than that of electrons, the interband differential conductivity increases, which also expands the region of the negative DT.

C. Influence of CH self-energy

Finally, we address the influence of the CH self-energy on the emergence of the negative DT (positive differential conductivity). The total differential conductivity with the CH self-energy for graphene on SiO_2 substrate in the electron-temperature–chemical-potential (T_e-μ_1) parameter spaces is plotted in Fig. 4(a). Here the probe-photon energy ω is chosen to be 1500 meV. Comparing with the results without the CH self-energy [Fig. 3(e)], one finds that the CH self-energy enhances both the region and the magnitude of the positive differential conductivity markedly. This means that the variation of the CH self-energy after the pumping is the dominant mechanism leading to the positive differential conductivity at such high ω if it is taken into consideration. It is worth noting that the shape for the region of the positive differential conductivity with the CH self-energy is similar to the one

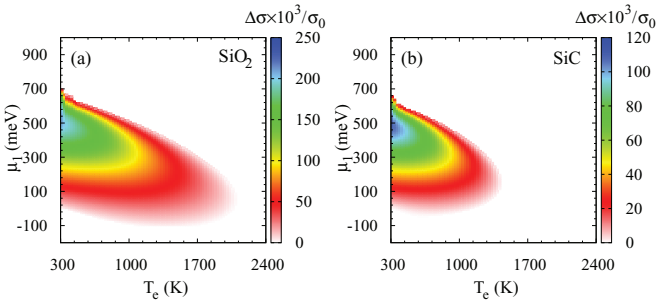

FIG. 4. (Color online) Total differential conductivity with the CH self-energy for graphene on SiO_2 (a) and SiC (b) in T_e-μ_1 parameter space. For clarity, only the positive differential conductivity is plotted.

without it [Fig. 3(e)] (this is also true for ω-μ_1 parameter space). This means that the tendency for the emergence of the total differential conductivity summarized in Sec. III B is still valid, although the variation of the CH self-energy after the pumping becomes the dominant mechanism leading to the positive differential conductivity.

It is noted that since the CH self-energy mainly comes from the variation of the screening, its influence should be smaller if the graphene layer is on a substrate with higher background dielectric consistent. To confirm this, we show the results for graphene on SiC [Fig. 4(b)], whose background dielectric constant is 2.2 times of that for SiO_2. One finds that both the magnitude and the region of the positive differential conductivity decrease obviously compared with the one on SiO_2 substrate. Nevertheless, the positive differential conductivity (negative DT) region shown on SiC substrate is still very large.

Actually, the negative DT region shown on SiO_2 and SiC substrates with the CH self-energy is so large that it disagrees with some of the existing experiments.[13,30,31] Dawlaty *et al.*[13] have shown experimentally for graphene on SiC substrate that the DT is positive when the optical excited electron density is about 10^{12} cm^{-2} with the corresponding T_e estimated to be around 900 K and μ_1 around zero under the probe-photon energy close to 1500 meV.[20] However, the numerically obtained DT with these parameters is negative as shown in Fig. 4(b). Moreover, Ruzicka *et al.*[30] and Brida *et al.*[31] also showed in graphene on SiO_2 substrate that the DT is positive when the excited electron density is about 10^{13} cm^{-2} with the corresponding T_e estimated to be around 1000 K and μ_1 around 350 meV.[30] However, the numerically obtained DT with the CH self-energy is also negative as shown in Fig. 4(a). Nevertheless, for the case without the CH self-energy, the DTs under these parameters are all positive [Fig. 3(e) for the SiO_2 substrate and that for the SiC substrate is not shown]. Further considering the fact that the result obtained without the CH self-energy is consistent with the experiment with the negative DT (Sec. III B),[24] one concludes that although the calculation of the CH self-energy used here is very successful in semiconductors,[39,40] it overestimates the Coulomb self-energy in the gapless graphene system. This may come from the approximations used to obtain Eq. (11). For example, the background dielectric constant κ is taken to be constant although it is shown to increase with q (Ref. 70) and the vertex correction[38] for the Coulomb screening is neglected. A better description on the influence of the Coulomb self-energy is beyond the scope of this investigation.

IV. SUMMARY

In summary, we have investigated the emergence of the negative DT by calculating the optical conductivity based on the linear response theory with the Keldysh Green function approach. In our calculation, the influences of the electron-phonon and electron-impurity scatterings as well as the Coulomb self-energy are explicitly included. We investigate the system with the photon-excited electron density much larger than the equilibrium one and show that the negative DT (or equivalently, the positive differential conductivity) can appear at low probe-photon energy ω (in the order of the scattering rate) or at high ω (much larger than the scattering rate).

For the low ω case, the negative DT is shown to mainly come from the large increase of the intraband conductivity due to the large variation of the electron distribution after the pumping. As for the high ω case, it is shown that the interband conductivity with only scattering can lead to the negative DT when the hot-electron temperature T_e is close to the equilibrium one and the chemical potential μ_1 is higher than the equilibrium chemical potential but considerably lower than $\omega/2$. Moreover, the intraband conductivity can further expand this region of the negative DT because it always tends to decrease DT if T_e and μ_1 increase after the pumping. Furthermore, in the temperature range usually estimated in the experiments (around 1000 K), the HF self-energy is also shown to be able to contribute to the negative DT by increasing the interband differential conductivity considerably when μ_1 is several hundred meV higher than the equilibrium one. This further expands the region of the negative DT at high ω. Nevertheless, the HF self-energy has little influence on the intraband conductivity and hence its effect on the negative DT at low ω can be neglected. In addition, we also show that if the phonon temperature is smaller than that of electrons, the interband differential conductivity is increased which also expands the region of the negative DT. Our numerical results are consistent with the ω dependence of the negative DT obtained experimentally by Shang *et al.*[24]

The influence of the CH self-energy is also investigated. We find that it markedly expands the region of the negative DT. However, this expansion is too large which makes the obtained region of the negative DT become incompatible with the existing experiments.[13,30,31] This means that the CH self-energy calculated with the well established approach in semiconductors[39,40] overestimates the Coulomb self-energy in the gapless graphene system. More investigation to take into account the high order correlation is needed.

ACKNOWLEDGMENTS

The authors would like to thank T. S. Lai for valuable discussions. This work was supported by the National Natural Science Foundation of China under Grant No. 11334014, the National Basic Research Program of China under Grant No. 2012CB922002, and the Strategic Priority Research Program of the Chinese Academy of Sciences under Grant No. XDB01000000.

*Corresponding author: mwwu@ustc.edu.cn

[1] P. Avouris, Z. Chen, and V. Perebeinos, Nat. Nanotech. **2**, 605 (2007).

[2] A. H. Castro Neto, F. Guinea, N. M. R. Peres, K. S. Novoselov, and A. K. Geim, Rev. Mod. Phys. **81**, 109 (2009).

[3] N. M. R. Peres, Rev. Mod. Phys. **82**, 2673 (2010).

[4] W. Choi, I. Lahiri, R. Seelaboyina, and Y. S. Kang, Crit. Rev. Solid State Mater. Sci. **35**, 52 (2010).

[5] F. Schwierz, Nat. Nanotech. **5**, 487 (2010).

[6] P. Avouris, Nano Lett. **10**, 4285 (2010).

[7] D. S. L. Abergel, V. Apalkov, J. Berashevich, K. Ziegler, and T. Chakraborty, Adv. Phys. **59**, 261 (2010).

[8] F. Bonaccorso, Z. Sun, T. Hasan, and A. C. Ferrari, Nat. Photon. **4**, 611 (2010).

[9] S. Das Sarma, S. Adam, E. H. Hwang, and E. Rossi, Rev. Mod. Phys. **83**, 407 (2011).

[10] A. F. Young and P. Kim, Annu. Rev. Condens. Matter Phys. **2**, 101 (2011).

[11] A. H. Castro Neto and K. Novoselov, Rep. Prog. Phys. **74**, 082501 (2011).

[12] V. N. Kotov, B. Uchoa, V. M. Pereira, F. Guinea, and A. H. Castro Neto, Rev. Mod. Phys. **84**, 1067 (2012).

[13] J. M. Dawlaty, S. Shivaraman, M. Chandrashekhar, F. Rana, and M. G. Spencer, Appl. Phys. Lett. **92**, 042116 (2008).

[14] D. Sun, Z.-K. Wu, C. Divin, X. Li, C. Berger, W. A. de Heer, P. N. First, and T. B. Norris, Phys. Rev. Lett. **101**, 157402 (2008).

[15] P. A. George, J. Strait, J. Dawlaty, S. Shivaraman, M. Chandrashekhar, F. Rana, and M. G. Spencer, Nano Lett. **8**, 4248 (2008).

[16] H. Choi, F. Borondics, D. A. Siegel, S. Y. Zhou, M. C. Martin, A. Lanzara, and R. A. Kaindl, Appl. Phys. Lett. **94**, 172102 (2009).

[17] R. W. Newson, J. Dean, B. Schmidt, and H. M. van Driel, Opt. Express **17**, 2326 (2009).

[18] M. Breusing, C. Ropers, and T. Elsaesser, Phys. Rev. Lett. **102**, 086809 (2009).

[19] P. Plochocka, P. Kossacki, A. Golnik, T. Kazimierczuk, C. Berger, W. A. de Heer, and M. Potemski, Phys. Rev. B **80**, 245415 (2009).

[20] H. Wang, J. H. Strait, P. A. George, S. Shivaraman, V. B. Shields, M. Chandrashekhar, J. Hwang, F. Rana, M. G. Spencer, C. S. Ruiz-Vargas, and J. Park, Appl. Phys. Lett. **96**, 081917 (2010).

[21] B. A. Ruzicka, L. K. Werake, H. Zhao, S. Wang, and K. P. Loh, Appl. Phys. Lett. **96**, 173106 (2010).

[22] J. Shang, Z. Luo, C. Cong, J. Lin, T. Yu, and G. G. Gurzadyan, Appl. Phys. Lett. **97**, 163103 (2010).

[23] L. Huang, G. V. Hartland, L. Chu Luxmi, R. M. Feenstra, C. Lian, K. Tahy, and H. Xing, Nano Lett. **10**, 1308 (2010).

[24] J. Shang, T. Yu, J. Lin, and G. G. Gurzadyan, ACS Nano **5**, 3278 (2011).

[25] S. Winnerl, M. Orlita, P. Plochocka, P. Kossacki, M. Potemski, T. Winzer, E. Malic, A. Knorr, M. Sprinkle, C. Berger, W. A. de Heer, H. Schneider, and M. Helm, Phys. Rev. Lett. **107**, 237401 (2011).

[26] P. J. Hale, S. M. Hornett, J. Moger, D. W. Horsell, and E. Hendry, Phys. Rev. B **83**, 121404(R) (2011).

[27] M. Breusing, S. Kuehn, T. Winzer, E. Malic, F. Milde, N. Severin, J. P. Rabe, C. Ropers, A. Knorr, and T. Elsaesser, Phys. Rev. B **83**, 153410 (2011).

[28] K. M. Dani, J. Lee, R. Sharma, A. D. Mohite, C. M. Galande, P. M. Ajayan, A. M. Dattelbaum, H. Htoon, A. J. Taylor, and R. P. Prasankumar, Phys. Rev. B **86**, 125403 (2012).

[29] T. Li, L. Luo, M. Hupalo, J. Zhang, M. C. Tringides, J. Schmalian, and J. Wang, Phys. Rev. Lett. **108**, 167401 (2012).

[30] B. A. Ruzicka, S. Wang, J. Liu, K.-P. Loh, J. Z. Wu, and H. Zhao, Opt. Mater. Express **2**, 708 (2012).

[31] D. Brida, A. Tomadin, C. Manzoni, Y. J. Kim, A. Lombardo, S. Milana, R. R. Nair, K. S. Novoselov, A. C. Ferrari, G. Cerullo, and M. Polini, Nat. Commun. **4**, 1987 (2013).

[32] K. J. Tielrooij, J. C. W. Song, S. A. Jensen, A. Centeno, A. Pesquera, A. Zurutuza Elorza, M. Bonn, L. S. Levitov, and F. H. L. Koppens, Nat. Phys. **9**, 248 (2013).

[33] N. M. R. Peres, F. Guinea, and A. H. Castro Neto, Phys. Rev. B **73**, 125411 (2006).

[34] B. Scharf, V. Perebeinos, J. Fabian, and P. Avouris, Phys. Rev. B **87**, 035414 (2013).

[35] B. Y. Sun and M. W. Wu, New J. Phys. **15**, 083038 (2013).

[36] P. N. Romanets and F. T. Vasko, Phys. Rev. B **81**, 085421 (2010).

[37] A. Altland and B. Simons, *Condensed Matter Field Theory* (Cambridge University Press, New York, 2010).

[38] G. D. Mahan, *Many-Particle Physics* (Plenum, New York, 1990).

[39] W. W. Chow and S. W. Koch, *Semiconductor-Laser Fundamentals: Physics of the Gain Materials* (Springer, Berlin, 1999).

[40] C. K. Choi, Y. H. Kwon, J. S. Krasinski, G. H. Park, G. Setlur, J. J. Song, and Y. C. Chang, Phys. Rev. B **63**, 115315 (2001).

[41] H. Haug and A.-P. Jauho, *Quantum Kinetics in Transport and Optics of Semiconductors* (Springer, Berlin, 1998).

[42] D. P. DiVincenzo and E. J. Mele, Phys. Rev. B **29**, 1685 (1984).

[43] B. Y. Sun, Y. Zhou, and M. W. Wu, Phys. Rev. B **85**, 125413 (2012).

[44] X. L. Lei and M. W. Wu, Mod. Phys. Lett. B **6**, 1935 (1992); Phys. Rev. B **47**, 13338 (1993).

[45] E. H. Hwang and S. Das Sarma, Phys. Rev. B **77**, 081412(R) (2008).

[46] Q. Li, E. H. Hwang, and S. Das Sarma, Phys. Rev. B **84**, 235407 (2011).

[47] J. Hwang, J. P. F. LeBlanc, and J. P. Carbotte, J. Phys.: Condens. Matter **24**, 245601 (2012).

[48] G. B. Ren and P. Blood, Phys. Rev. B **60**, 16675 (1999).

[49] F. Rana, IEEE Trans. Nanotechnol. **7**, 91 (2008).

[50] J. M. Dawlaty, S. Shivaraman, J. Strait, P. George, M. Chandrashekhar, F. Rana, M. G. Spencer, D. Veksler, and Y. Chen, Appl. Phys. Lett. **93**, 131905 (2008).

[51] L. A. Falkovsky, J. Phys.: Conf. Ser. **129**, 012004 (2008).

[52] T. Winzer, A. Knorr, and E. Malic, Nano Lett. **10**, 4839 (2010).

[53] R. Kim, V. Perebeinos, and P. Avouris, Phys. Rev. B **84**, 075449 (2011).

[54] T. Winzer and E. Malić, Phys. Rev. B **85**, 241404(R) (2012).

[55] T. Winzer, E. Malić, and A. Knorr, Phys. Rev. B **87**, 165413 (2013).

[56] E. Malic, T. Winzer, E. Bobkin, and A. Knorr, Phys. Rev. B **84**, 205406 (2011).

[57] B. Wunsch, T. Stauber, F. Sols, and F. Guinea, New J. Phys. **8**, 318 (2006).

[58] M. Müller, L. Fritz, and S. Sachdev, Phys. Rev. B **78**, 115406 (2008).

[59] J. González, F. Guinea, and M. A. H. Vozmediano, Phys. Rev. Lett. **77**, 3589 (1996).

[60] D. V. Khveshchenko, Phys. Rev. B **74**, 161402 (2006).

[61] B. Tanatar, J. Phys.: Condens. Matter **8**, 5997 (1996).

[62] H. Haug and S. W. Koch, *Quantum Theory of the Optical and Electronic Properties of Semiconductors*, 4th ed. (World Scientific, Singapore, 2004).

[63]A. Joshua and V. Venkataraman, Phys. Rev. B **77**, 085202 (2008).
[64]M. I. Katsnelson, K. S. Novoselov, and A. K. Geim, Nat. Phys. **2**, 620 (2006).
[65]This can be seen directly from Eq. (5) by replacing the electron spectral function $A(\mathbf{k},\eta,\omega)$ by a Lorentzian.
[66]R. Bistritzer and A. H. MacDonald, Phys. Rev. Lett. **102**, 206410 (2009).
[67]J. C. W. Song, M. S. Rudner, C. M. Marcus, and L. S. Levitov, Nano Lett. **11**, 4688 (2011).
[68]D. Sun, G. Aivazian, A. M. Jones, J. S. Ross, W. Yao, D. Cobden, and X. Xu, Nat. Nanotechnol. **7**, 114 (2012).
[69]T. Low, V. Perebeinos, R. Kim, M. Freitag, and P. Avouris, Phys. Rev. B **86**, 045413 (2012).
[70]J. Lischner, D. Vigil-Fowler, and S. G. Louie, Phys. Rev. Lett. **110**, 146801 (2013).